PUC Minas
A B A K Ó S
Instituto de Ciências Exatas e Informática

Non-extensive entropy algorithm for multi-region segmentation: generalization and comparison*

Algoritmo de entropia não-extensiva para segmentação de multi-região: generalização e comparação

Paulo Sergio Rodrigues[1]
Gilson Antonio Giraldi[2]

Abstract

Since eighties, the concept of entropy has been applied in the field of image processing and analysis. This concept is based on Shannon entropy which is an application in the Theory of Information of the traditional Boltzmann-Gibbs entropy, proposed to the classical thermodynamic. For decades, it is known that this old formalism of entropy fails to explain some physical system if they have complex behavior such as long-rang and long-memory interactions. Recently, studies in mechanical statistics have proposed a new kind of entropy, called Tsallis entropy (or q-entropy or non-extensive entropy), which has been considered with promising results on several application in order to explain such phenomena. In this paper we proposed an algorithm for image segmentation which is based on this new kind of entropy. Our approach, called Non-Extensive Segmentation Recursive Algorithm (NESRA) is an extension of other previous methodologies to binarize images only. In order to show the robustness of the NESRA performance, we compare it with well known and traditional approaches such as bootstrap, fuzzy c-means, k-means, self-organizing map and watershed image clustering methods. We show that, in several cases, the NESRA is better or overcomes these traditional approaches in distinct class of images.

Keywords: Tsallis entropy. Image segmentation. Non-extensive entropy.

*Artigo convidado.

[1]Centro Universitario da FEI, São Bernardo do Campo, SP, Brasil, Grupo de Processamento de Sinais e Imagens, psergio@fei.edu.br
[2]Laboratório Nacional de Computação Científica, Petrópolis, RJ, Brasil, gilson@lncc.br

Resumo

Desde os anos oitenta, o conceito de entropia tem sido aplicado na área de processamento de imagens. Este conceito baseia-se na entropia de Shannon, que é uma aplicação da Teoria da Informação da tradicional entropia Boltzmann-Gibbs, proposta no campo da termodinâmica clássica. No entanto, há décadas sabe-se que este antigo formalismo não consegue explicar alguns sistemas físicos se eles têm um comportamento complexo tal como interações de longo alcance espacial e temporal, bem como, comportamento fractal sob certas condições muito específicas. Recentemente, estudos em mecânica estatística têm proposto um novo tipo de entropia, chamada entropia de Tsallis (q-entropia ou entropia não-extensiva), cujos resultados têm sido considerados promissores em diversas aplicações, principalmente para explicar tais fenômenos. Neste trabalho, foi proposto um algoritmo para segmentação de imagens que se baseia neste novo tipo de entropia. A abordagem proposta aqui, chamada de Algoritmo Recursivo de Segmentação Não-Extensiva (NESRA, do inglês), é uma extensão de outras metodologias anteriores cujo objetivo é binarizar imagens digitais. A fim de mostrar a robustez do desempenho do NESRA, comparamos esse algoritmo com abordagens bem conhecidas e tradicionais, como *bootstrap, fuzzy c-means, k-means, self-organizing maps e watershed clustering*. Mostramos que, em vários casos, o NESRA é melhor ou supera essas abordagens tradicionais em classes distintas de imagens.

Palavras-chave: Entropia de Tsallis. Segmentação de imagens. Entropia não-extensiva.

1 INTRODUCTION

Image segmentation plays an important role on the basis of most of all computational vision systems. In order to accomplish automatically tasks such as scene recognition, for instance, a software needs initially to separate the scene into salient regions. This is similar to extract homogeneous regions from the background considering particular features.

Regarding the large volume of algorithms designed to accomplish the whole task of image segmentation, we can note two main groups: those designed for the primary task of region clustering according to local features and those composed of small procedures. These small procedures generally post-process the output of the first group's algorithms in order to finer segmentation. For example, after a initial segmentation, we can use some criterion to merge or split coherent regions. In this paper, we call the algorithms of the first group of basic segmentation algorithms (or simple basic algorithms). Among them, we can highlight examples such as the well known k-means, ISODATA, mean-shift, fuzzy c-means, bootstrap, SOM, watershed and several others based on histograms, just to name a few. From the second group, we can cite the works of Makrogiannis, Economou and Fotopoulos (2005), Makrogiannis et al. (2005) and Pappas (1992).

In order to minimize the computational time carried out by the second group, the first group's basic algorithms must be improved as much as possible. This is one of the main reasons for which the focus of this paper is on the first group.

The k-mean (GRAY; LINDE, 1982) and ISODATA (LOHMANN, 1998) are widely used clustering techniques proved to be optimal. However, they suffer the problems of local optima, clustering reproducibility and initialization sensitivity. Also, they require the number of clusters to be known *a priori*. Works using K-mean algorithm focusing on image clustering can be seen in (SINGH et al., 1996; CHEN; LUO; PARKER, 1998; LUO; YU-FEI; HONG-JIANG, 2003).

The mean-shift algorithm is a general nonparametric technique proposed by Comaniciu and Meer (2002) for clustering of complex multimodal feature space. It randomly tessellates the space with search windows, and moves until convergence is achieved at the nearest mode of the underlying probability distribution of density gradients. Several application of this algorithm for color clustering can also be found in (XIAN-JIU; WEI, 2005; LUO; KHOSHGOFTAAR, 2004; RONG-CHUN, 2003).

Bootstrap clustering technique is similar to other resamplig schemes, such as cross-validation and jackknifing. A bootstrap is obtained by sampling with replacement from an empirical distribution function from training set. Chen et al. (2002) applied a bootstrap implementation to computer-aided diagnosis in breast ultrasound images. Dutendas et al. (1994) presented an Bayesian approach combined with a bootstrap algorithm in order to segment images from the retina. Another two applications applying bootstrap techniques on image segmentation can be found in (ZHENG; XIAN-BIN; WEI, 2004; MARSHALL, 1996).

The Watershed transform is a reliable tool for initial image segmentation. A significant advantage of Watershed segmentation and a reason behind its extended utilization is that

boundaries on the image plane are always guaranteed to be connected and closed, and each gradient minimum corresponds to one region (MEYER, 1992). A nice explaning about Watershed algorithm can be found also in (GONZALEZ; WOODS, 1992).

As an unsupervised clustering algorithm we can cite the Fuzzy c-mean (FCM) which has been applied successfully to a number of problems involving feature analysis, clustering and classifier design. It has been applied to wide variety of applications such as agricultural engineering, astronomy, chemistry, geology, image analysis, medical diagnosis, shape analysis and target recognition (BEZDEK, 1987). Unlabeled data are classified by definition of a norm, cluster prototype and by minimizing an objective function. Although the description of the original algorithm dates back from 1973 (BEZDEK, 1973; DUNN, 1974), derivatives have been described with modified definitions for the norm and prototypes for the cluster center (KRISHNAPURAM; NASRAOUI; KELLER, 1992; DAVE; BHASWAN, 1992).

One of the most used methods in the last years to image clustering is the so called self organizing maps (SOM), proposed by Kohonen (1989). The SOM neural network consists of two layers, and for every neuron in the input layer, there is a link to every neuron in the output layer. During the training process of SOM network, for each input vector we get one best matching neuron in the output layer. Here a competitive learning algorithm is used to adjust weight vectors in the neighborhood of best matching neuron. The adjustment decreases as the time and the range of neighborhood increases. The following are interest works on this line.

Generally, several algorithms for clustering are combined with other approaches in order to reach finer results. Dong and Xie 2005 present a comparison between several SOM networks for clustering color images. Li and Li (2003), presented a combination of SOM and fuzzy systems for segmentation of several color images. Rickard et al. (2004) use a SOM network applied two times at the same set of images in order to segment mammographic images. The first application intends to achieve a initial segmentation and the second intends to finer segmentation. Goktepe, Yalabik and Atalay 1996 use a SOM combined with a multilayer SOM (Hierarchical SOM - HSOM) in order to sement textured images. Kurnaz, Dokur and Olmez (2001) use a called Incremental SOM (ISOM) neural network in order to segment ultrasound images where elements of feature vectors are formed by the Fast Fourier Transformation (FFT) of image intensities in a 4x4 blocs. They compare the traditional SOM with the proposed ISOM and report better results.

Shah-Hosseini and Safabakhsh (2002) proposed a growing time adaptative SOM (called TASOM) followed by a post-processing algorithm which recognizes each peak neuron along with its left and right limits. This way, the number of regions, and the regions themselves are determined. These properties, in fact, make the proposed segmentation algorithm an automatic multilevel thresholding algorithm. In their work, each neuron in a TASOM network has its own learning rate and neighborhood function which are updated automatically with the incoming input vectors. Also, the TASOM has a growing number of neurons. A combination of SOM and Probabilistic Neural Network (PNN) has also be proposed, like Ma et al. (1998) which presented a SOM combined with a PNN in order to segment large volume data of CT images.

Image segmentation is a processing inherently cognitive, thereby concerning the brain. As such, it is a subjective task, yielding to an oversegmented scene (with high level of details) or an undersegmented one (with high level of abstraction). Normally, there is a high correlation between the low level features and the high level ones. These correlations are not necessarily linear and there are few researches regarding them. An exception is the work of Albuquerque et al. (2004), which have used a new kind of entropy, called Tsallis non-extensive entropy (TSALLIS, 1999), in order to segment mammography gray scale images. They have achieved better results than the traditional Boltzmann-Gibbs entropy when the input images are considered as having high interactions between features. However, their algorithm only binarize gray scale images according to non-extensive theory. Also, they have tested their algorithm only over a small data set. Then, it is interesting to see how the Tsallis entropy, also called q-entropy, behaves applying it over more natural images and comparing the results with other approaches for the same purpose.

In this paper, we propose an extension of the algorithm presented by Albuquerque et al. (2004) applying recursively the q-entropy over the input image. In order to show the robustness of our method, we also compare it with well known basic approaches under several class of images.

The paper is organized as follows. In Section 2, we introduce the q-entropy under the context of non-extensive systems and explains the original non-recursive method. In Section 3, we compare the proposed algorithm with other methodologies. Finally, in Section 4 we discuss the results and make some conclusions.

2 THE PROPOSED METHOD

2.1 Tsallis Entropy

The entropy is an idea born under the thermodynamics concept, not as something mainly intuitive, but as something mainly quantitative, defined by an equation. Also, we may say that it is a concept that is associated to the order of irreversible processes in the universe. Physically, it may be associated to the amount of disorder in a physical system. Shannon redefined the concept of entropy of Boltzmann-Gibbs as an uncertainty measure associated to the content of information of a system. In this theory, the entropy of a discrete source is often obtained from a probability distribution $P = (p_1, \ldots, p_k)$, $0 \leq p_i \leq 1$ and $\sum_i p_i = 1$, where p_i is the probability of finding the system in the state i. In this context, the Shannon entropy (BGS) may be described as

$$S = -\sum_i p_i \ln(p_i) \tag{1}$$

Generically speaking, systems that have statistics of the type BGS are called extensive systems. Such systems have an additive property, defined as follows. Let P and Q be two

random variables, with probability densities functions $P = (p_1, \ldots, p_n)$ and $Q = (q_1, \ldots, q_m)$, respectively. If P and Q will be independent, under the context of the Probability Theory, the entropy of the composed distribution[1] verify the so called additivity rule:

$$S(P * Q) = S(P) + S(Q) \tag{2}$$

This traditional form of entropy, called Boltzmann-Gibbs-Shannon (BGS) entropy, is well known and for years has achieved relative success to explain several phenomenon *if* the effective microscopic interactions are *short*-ranged (i.e., close spatial connections) *and* the effective spatial microscopic memory is *short*-ranged (i.e., *close* time connections) *and* the boundary conditions are *non(multi)fractal*. Roughly speaking, the standard formalism are applicable whenever (and probably only whenever) the relevant space-time (hence the relevant phase space) is non(multi)fractal. If this is not the case, some kind of extension appears to became necessary, as said Tsallis (1999):

> [...] In complete analogy with Newtonian mechanics, when it becomes only an approximation (an increasingly bad one) when the involved velocities approach that of light or the masses are as small as say the electron mass; the standard statistical mechanics do not apply when the above requirements (short-range microscopic interactions, short-ranged microscopic memory and (multi)-fractal boundary conditions) are not the case [...].

However, recent developments, based on the concept of nonextensive entropy, also called Tsallis entropy, have generated a new interest in the study of Shannon entropy for Information Theory (TSALLIS, 2001; SHANNON; WEAVER, 1948; ALBUQUERQUE et al., 2004). This interest appears mainly due to the similarities between the functions of Shannon-Boltzmann-Gibbs entropy. Tsallis entropy (or q-entropy) is a new proposal for the generalization of Boltzmann-Gibbs traditional entropy applied to nonextensive physical systems.

The non-extensive characteristic of Tsallis entropy has been applied through the inclusion of a parameter q, which generates several mathematical properties such as non-negativity, concavity, equiprobability, q-additivity and q-axiomality of group. The general equation of entropy proposed by Tsallis, is as follows:

$$S_q(p_1, \ldots p_k) = \frac{1 - \sum_{i=1}^{k} (p_i)^q}{q - 1} \tag{3}$$

where k is the total number of possibilities of the system and the real number q is the entropic index that characterizes the degree of non-extensiveness. In the limit $q \to 1$, Equation (3) meets the traditional BGS entropy defined by Equation (1).

These characteristics give to q-entropy flexibility in explanation of several physical systems. On the other hand, this new kind of entropy does not fail to explain the traditional physical systems since it is a generalization.

[1] we define the composed distribution, also called direct product of $P = (p_1, \ldots, p_n)$ and $Q = (q_1, \ldots, q_m)$, as $P * Q = \{p_i q_j\}_{i,j}$, with $1 \leq i \leq n$ and $1 \leq j \leq m$

However, a generalization of some theory may suppose the violation of one of its postulates. In the case of the generalized entropy proposed by Tsallis, the additive property described by Equation (2) is violated in the form of Equation (4), which applies if the system has a non-extensive characteristic. In this case, the Tsallis statistics is useful and the q-additivity describes better the composed system. In our case, the experimental results (Section 3) show that it is better to consider our systems as having non-extensive behavior.

$$S_q(P+Q) = S_q(P) + S_q(Q) + (1-q) \cdot S_q(P) \cdot S_q(Q). \tag{4}$$

In this equation, the term $(1-q)$ stands for the degree of non-extensiveness: similarly as Equation (3), in the limit $q \to 1$, $S(P*Q)$ meets the the BGS entropy.

Considering $S_q \geq 0$ in the pseudo-additive formalism of the Equation (4), the following classification for entropic systems is defined:

- Subextensive entropy $(q > 1)$
  $S_q(P+Q) > S_q(P) + S_q(Q)$
- Extensive entropy $(q = 1)$
  $S_q(P+Q) = S_q(P) + S_q(Q)$
- Superextensive entropy $(q < 1)$
  $S_q(P+Q) < S_q(P) + S_q(Q)$

Taking into account the similarities between the formalisms of Boltzmann-Gibbs-Shannon entropy, it is interesting to investigate the possibility of the generalization of Shannon entropy to the case of the information theory, as has been recently shown by Yamano (2001). This generalization may be extended to image segmentation tasks, by applying Tsallis entropy, which has nonadditive information contents.

In this paper we propose to segment an image using q-entropy and compare it with other well known segmentation approaches. The motivations to use the q-entropy are: 1) managing only a simple parameter q opens the possibility of simply applying several segmentation and choosing that generates the best result; 2) as suggested in (ALBUQUERQUE et al., 2004), the mammographic images and possible several others natural images have a non-extensive behavior; 3) it is simple and makes the implementation easy having a low computational overload.

The contributions of our paper are: 1) proposing a recursive algorithm from that proposed in (ALBUQUERQUE et al., 2004); 2) applying the non-extensive segmentation for a multi-region segmentation task; 3) compare the non-extensive approach against other prominent methodologies; and 4) applying our method on a large range class of images.

2.2 The Non-extensive multi-region segmentation algorithm (NESRA)

Applying the concept of entropy in order to segment a digital image is a common practice since Pun (1981) showed that to maximize the foreground and background's Shannon entropy of a gray level image may reach good results concerning the prominent regions. Then, other works following the same line were proposed, e.g, Kapur, Sahoo and Wong (1985) maximized un upper bound of the total *a posteriori* entropy in order to obtain the threshold level. Abutaleb (1989) extended the method using two-dimensional entropies. Li and Lee (1993), and Pal (1996) used the directed divergence of Kullback for the selection of the threshold, and Soltani and Wong (1988) used the Reiny entropy model for image thresholding.

In 2004, Albuquerque et al. (2004) presented the concept of non-extensive entropy applied to mammographic gray scale images. They assume a probability distribution, one for background and other for foreground and take the threshold that maximizes the non-additivity characteristic given by Equation (4). However, as several methods designed to produce binary images, this approach does not work for multi-region segmentation as well. Then, we proposed an extension of the method presented in Albuquerque et al. (2004) applying recursively the maximization of Equation (4) over the background and the foreground in order to achieve multi-regions of homogenous gray level or color distribution.

It can be argued that any parametric or non parametric method with the objective of finding an ideal threshold, producing a binary image, can be recursively used in the foreground and in the background in order to achieve multi-regions. However, our approach, based on non-extensive entropy, out performs several well known approaches under the same conditions. In this section, we show our new multi-region segmentation method based also on the non-extensive entropy concept.

First of all, we will review the non-extensive approach for image segmentation proposed in (ALBUQUERQUE et al., 2004).

2.3 Non-extensive segmentation algorithm for image binarization

Suppose an image with k gray-levels, let the probability distribution of these levels be $P = \{p_i = p_1; p_2; \ldots; p_k\}$. Now, we want to consider two probability distribution from P, one for the foreground (P_A) and another for the background (P_B). We can make a partition between the pixels from P into A and B. In order to maintain the constraints $0 \leq P_A \leq 1$ and $0 \leq P_B \leq 1$ we must re-normalize both distribution as:

$$P_A : \frac{p_1}{p_A}, \frac{p_2}{p_A}, \ldots, \frac{p_t}{p_A} \tag{5}$$

$$P_B : \frac{p_{t+1}}{p_B}, \frac{p_{t+2}}{p_B}, \ldots, \frac{p_k}{p_B} \tag{6}$$

where $p_A = \sum_{i=1}^{t} p_i$ and $p_B = \sum_{i=t+1}^{k} p_i$.

Now, we calculate the *a priori* Tsallis entropy for each distribution such as

$$S_A = \frac{1 - \sum_{i=1}^{t} (\frac{p_i}{p_A})^q}{q-1} \tag{7}$$

$$S_B = \frac{1 - \sum_{i=t+1}^{k} (\frac{p_i}{p_B})^q}{q-1} \tag{8}$$

We can observe that the Tsallis entropy represented by Equations (3), (7) and (8), depends on directly the parameter t for the foreground and background, and it is formulated as the sum of each entropy, allowing the pseudo-additive property for statistically independent systems, defined in Equation (9).

$$S_{A+B}(t) = \frac{1 - \sum_{i=1}^{t} (p_A)^q}{q-1} + \frac{1 - \sum_{i=t+1}^{k} (p_B)^q}{q-1} + (1-q).\frac{1 - \sum_{i=1}^{t} (p_A)^q}{q-1}.\frac{1 - \sum_{i=t+1}^{k} (p_B)^q}{q-1} \tag{9}$$

To accomplish the segmentation task, Albuquerque et al. (2004) maximizes the information measure between the two classes (foreground and background). When $S_{A+B}(t)$ is maximized, the luminance level t is considered to be the optimum threshold value, t_{opt}. This can be achieved with a cheap computational effort of

$$t_{opt} = argmax[S_A(t) + S_B(t) + (1-q).S_A(t).S_B(t)] \tag{10}$$

Note that the value t which maximizes Equation (10) depends on mainly the parameter q. This is an advantage due to its simplicity. Therefore, varying q it is possible to obtain a value of t adapted to current illumination conditions, for example. In this paper, we will show experimentally that the range of values set to q while looking for a value of t which maximizes Equation (10) is small. It makes the non-extensive approach adequate to applications that need segmentation at real time. In our work we use the simple idea of varying q from a subextensive space to a superextensive one. In the next section, we present the recursive formulation for this algorithm.

2.4 Non-extensive segmentation recursive algorithm for multi-region image segmentation

Following the definitions and formulations from the last section, we can take each distribution P_A and P_B and subdivide them into two news distribution, P_{A1}, P_{A2}, P_{B1} and P_{B2}, as following:

$$P_{A1} : \frac{p_1}{p_{A1}}, \frac{p_2}{p_{A1}}, \ldots, \frac{p_t}{p_{A1}} \tag{11}$$

$$P_{A2} : \frac{p_{t+1}}{p_{A2}}, \frac{p_{t+2}}{p_{A2}}, \ldots, \frac{p_{\varrho}}{p_{A2}} \tag{12}$$

$$P_{B1} : \frac{p_{\varrho+1}}{p_{B1}}, \frac{p_{\varrho+2}}{p_{B1}}, \ldots, \frac{p_{\upsilon}}{p_{B1}} \tag{13}$$

$$P_{B2} : \frac{p_{\upsilon+1}}{p_{B2}}, \frac{p_{\upsilon+2}}{p_{B2}}, \ldots, \frac{p_{k}}{p_{B2}} \tag{14}$$

and having the constraints $p_{A1} = \sum_{i=1}^{t} p_i, p_{A2} = \sum_{t+1}^{\varrho} p_i, p_{B1} = \sum_{\varrho+1}^{\upsilon} p_i, p_{B2} = \sum_{\upsilon+1}^{k} p_i$. For each one of these four above distributions we can compute its respective non-extensive entropy as follows:

$$S_{A1} = \frac{1 - \sum_{i=1}^{t} (\frac{p_i}{p_{A1}})^q}{q-1} \tag{15}$$

$$S_{A2} = \frac{1 - \sum_{i=t+1}^{\varrho} (\frac{p_i}{p_{A2}})^q}{q-1} \tag{16}$$

$$S_{B1} = \frac{1 - \sum_{i=\varrho+1}^{\upsilon} (\frac{p_i}{p_{B1}})^q}{q-1} \tag{17}$$

$$S_{B2} = \frac{1 - \sum_{i=\upsilon+1}^{k} (\frac{p_i}{p_{B2}})^q}{q-1} \tag{18}$$

Using Equations (4), (15) and (16) to compute $S(A) = S(A1 + A2)$ and, similarly (17) and (18) to compute $S(B) = S(B1 + B2)$, we have:

$$\begin{aligned} S_q(A+B) = \\ (\frac{1 - \sum_{i=1}^{t} (\frac{p_i}{p_{A1}})^q}{q-1} + \frac{1 - \sum_{i=t+1}^{\varrho} (\frac{p_i}{p_{A2}})^q}{q-1} + (1-q) \cdot \frac{1 - \sum_{i=1}^{t} (\frac{p_i}{p_{A1}})^q}{q-1} \cdot \frac{1 - \sum_{i=t+1}^{\varrho} (\frac{p_i}{p_{A2}})^q}{q-1}) + \\ (\frac{1 - \sum_{i=\varrho+1}^{\upsilon} (\frac{p_i}{p_{B1}})^q}{q-1} + \frac{1 - \sum_{i=\upsilon+1}^{k} (\frac{p_i}{p_{B2}})^q}{q-1} + (1-q) \cdot \frac{1 - \sum_{i=\varrho+1}^{\upsilon} (\frac{p_i}{p_{B1}})^q}{q-1} \cdot \frac{1 - \sum_{i=\upsilon+1}^{k} (\frac{p_i}{p_{B2}})^q}{q-1}) + \\ (1-q) \cdot \\ (\frac{1 - \sum_{i=1}^{t} (\frac{p_i}{p_{A1}})^q}{q-1} + \frac{1 - \sum_{i=t+1}^{\varrho} (\frac{p_i}{p_{A2}})^q}{q-1} + (1-q) \cdot \frac{1 - \sum_{i=1}^{t} (\frac{p_i}{p_{A1}})^q}{q-1} \cdot \frac{1 - \sum_{i=t+1}^{\varrho} (\frac{p_i}{p_{A2}})^q}{q-1}) \cdot \\ (\frac{1 - \sum_{i=\varrho+1}^{\upsilon} (\frac{p_i}{p_{B1}})^q}{q-1} + \frac{1 - \sum_{i=\upsilon+1}^{k} (\frac{p_i}{p_{B2}})^q}{q-1} + (1-q) \cdot \frac{1 - \sum_{i=\varrho+1}^{\upsilon} (\frac{p_i}{p_{B1}})^q}{q-1} \cdot \frac{1 - \sum_{i=\upsilon+1}^{k} (\frac{p_i}{p_{B2}})^q}{q-1}) \end{aligned} \tag{19}$$

In this case, to find the optimal luminance level, such as the equivalent in the Equation (10), we can compute the Equation (19) taken the argument that maximizes the next expression:

$$\begin{aligned} t_{opt} = argmax[(S_{A1} + S_{A2} + (1-q) \cdot S_{A1} \cdot S_{A2}) \cdot (S_{B1} + S_{B2} + (1-q) \cdot S_{B1} \cdot S_{B2}) \cdot (1-q) \\ \cdot (S_{A1} + S_{A2} + (1-q) \cdot S_{A1} \cdot S_{A2}) \cdot (S_{B1} + S_{B2} + (1-q) \cdot S_{B1} \cdot S_{B2})] \end{aligned} \tag{20}$$

The Equation (19) is simple, although with several terms. By developing a third recursion would yielding the number of terms up to sixteen, letting comprehension so much complex.

However, two observations may be done. First, the experimental results show that it is not necessary more than two or three recursions in order to obtain results which are equals or better than traditional methods. Second, the growing of the number of recursion does not enlarge the algorithm complexity or computation, since this growing accompanies a dropping of states to be computed at each recursion, like in the algorithms for binary partitions.

The recursive algorithm for the previous formulation is simple and we give it in the following.

Algorithm 1: Non-Extensive Segmentation Recursive Algorithm, NESRA procedure

Input: H = image histogram, i = first histogram bin, k = last histogram bin
Call NESRA(H, i, k) procedure

if Histogram H is homogeneous **then**
  Goto FIM
end if

for all $t = i$ until k **do**

  compute normalization for background
  compute normalization for foreground
  compute q-entropy for background according to Equation (7)
  compute q-entropy for foreground according to Equation (8)
  compute composed q-entropy according to Equations (9) and (10)
end for
$topt$ = argmax of the composed q-entropy
Call NESRA($H, i, topt$) procedure
Call NESRA($H, topt + 1, k$) procedure
FIM: there is nothing to do, return to calling procedure

In the next section, we apply the NESRA algorithm on several class of color and gray scale images. When the input are color images, we convert to gray scale. First, we apply our approach and finish comparing the results with five well known segmentation methods, namely: k-means, fuzzy c-means, watershed, SOM and bootstrap methodology. Since all method, including the NESRA procedure, can be set to achieve a random number of clusters, we ran all of them to find between 3 to 5 mainly regions, in order to compare them. We can note that 3 to 5 regions are sufficient for most of images in order to find mainly salient regions.

3 EXPERIMENTAL RESULTS

To show the robustness of our proposed multi-region segmentation algorithm as well as the range of its application, we have experimented it over several classes of complex color and gray scale images. Then, five images have been chosen: general scenes, human head tomography, object with homogeneous background, lenna and a paint image.

The images from general scenes in turn may be divided into 13 or 14 classes such as urban, animals under their environment, aircraft, sunset, cars, etc. The Fig. 1a is a random example. This class of images has unexpected feature colors and object combination under complex background since it was taken with a free photographic camera. Then, it is suitable to test our proposed algorithm.

Medical images applications have been a source of scientific investigation with several open challenges too, which demand for well segmentation algorithms. Therefore, we have chosen two class of well known medical images to test the robustness of our proposing: mamographic and magnetic resonance images (MRI). Mamography exams has been a valuable tool in breast cancer diagnosis as the cancer diseases are currently among the main cause of women death in the world. Besides, most of the 70% breast exams are carried out with a 2D scanner device and not with a more reliable 3D one. However, mammographic images (Fig. 1d is an example) have as main characteristics high speckle noises, low resolution, so many spurious regions and bed region of interest definition, demanding for specific algorithms. Then, it also is suitable to test any algorithm for image segmentation.

On the other hand, the MRI of human heads (Fig. 1g is an example) has been so far object of study for several years since MRI exams have becoming a valuable tool for cerebral cancer diagnosis as well as for cranio-facial prothesys reconstruction in case of skull deformation due to accidents, urban or home violence and congenital diseases. In the general case, the traditional prothesis design, manually built, has been gradually substituted by a 3D model manipulation which starts with a sequence of slices from a MRI exam followed by digital image processing application. Then, it is interesting to see the performance of our proposed algorithm under this well known and useful class of medical images.

The final class of images we will present our segmentation algorithm is the Columbia database (Figs. 1d is a random example). The photos of this database were taken under controlled light and viewer camera viewer. It is subdivided into 100 classes of daily objects. Each one with 72 views rotated as 5 degrees starting at 0 and ending on 360 degrees. Even all the images from this database have homogeneous black background, which facilitates the segmentation task, the target object shape and colors are complex which yields to complications when extracting the regions of interest.

Also, we have tasted our algorithm over the well known and used in digital image processing approaches lenna image, as it is interesting to meet our proposed algorithm to other similar approaches. We have included into our test a paint image, as it has high spackle noise distribution and is not natural, Fig. 1f.

All experiments were carried-out under three different values of q in the Equation (19): $0, 0.5$ and 1.0. These values were chosen in order to enclose the superextensive range as well as the extensive one. Then, when $q < 1$ we are considering the probability distribution as a superextensive system, as proposed by C. Tsallis, and when $q = 1.0$ we are considering the probability distribution as an extensive system regarding the Shannon traditional entropy. It allows facing segmented images as being superextensive systems against those segmented as

being subextensive ones. Instead of showing, that an image segmented with some range of q is better or worst each other (as it was just showed in Albuquerque et al. (2004) for mammographic images), we want to show mainly that our experiments with our recursive proposed algorithm, clearly outperforms the later results when the range is $q \leq 1$. For values out of this range, we will not present the results as it is very probable that the results will be better.

Figure 2 presents a set of three images which were segmented with the Tsallis entropy (non-recursive) (images a-c) for values of $q = 0, 0.5$ and 1.0, respectively. The original image is that of Fig. 1a (sunset). Clearly, this image has five main regions: the solar circumference, the solar crown, the sky, mountains and buildings. However, only two regions were found by the algorithm: with threshold $t = 105$, $q = 0$ (Fig. 2a); $t = 104$, $q = 0.5$ (Fig. 2b), and $t = 99$, $q = 1.0$ (Fig. 2c).

When we used our proposed recursive algorithm (NESRA), three more regions were outlined and the results, under the same q values, are clearly better. The Fig. 2d shows four regions which were found with threshold $t = \{105, 142, 58\}$, all for $q = 0$. Similarly, Fig. 2e shows four regions found with threshold $t = \{104, 139, 58\}$, all with $q = 0.5$; and Fig. 2f shows four regions found with threshold $t = \{99, 134, 56\}$, for $q = 1.0$.

Figure 1 – Six images used in our experiments.

(a) sunset (b) breast tumor (c) MRI

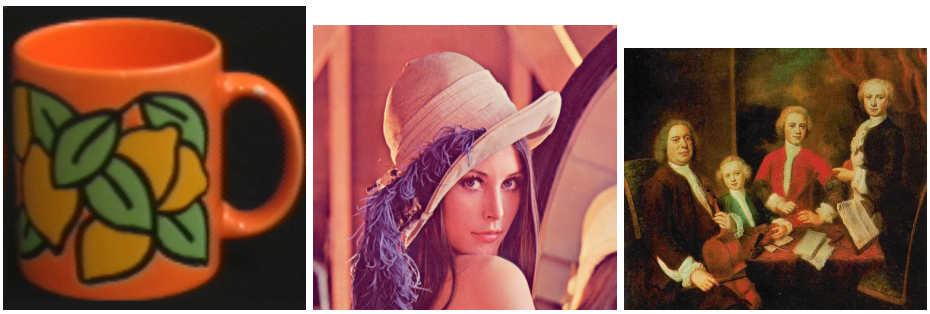

(d) simple object (e) lenna (f) paint

Subjectively speaking, the results when $q = 1.0$ (extensive systems) seems to be slightly better than when $q \neq 1.0$ (non-extensive systems) since it presents less noise and spurious regions. Then, it suggests an extensiveness of the system.

The next data set we have used in our experiments is the MR images. As aforementioned, MRI has been a valuable tool for several medical applications. Among them, we can outline mainly the head tumor diagnosis in hard and soft tissues. Then, since both MRI and CT exams can help 3D reconstruction of cranio, face and brain, these are indispensable tools when

Figure 2 – Sunset segmented image of Fig. 1a: with Tsallis entropy non-recursive algorithm (a-c) and with our extended proposed algorithm (NESRA) (d-f) for three different q values and two recursions. t stands for threshold.

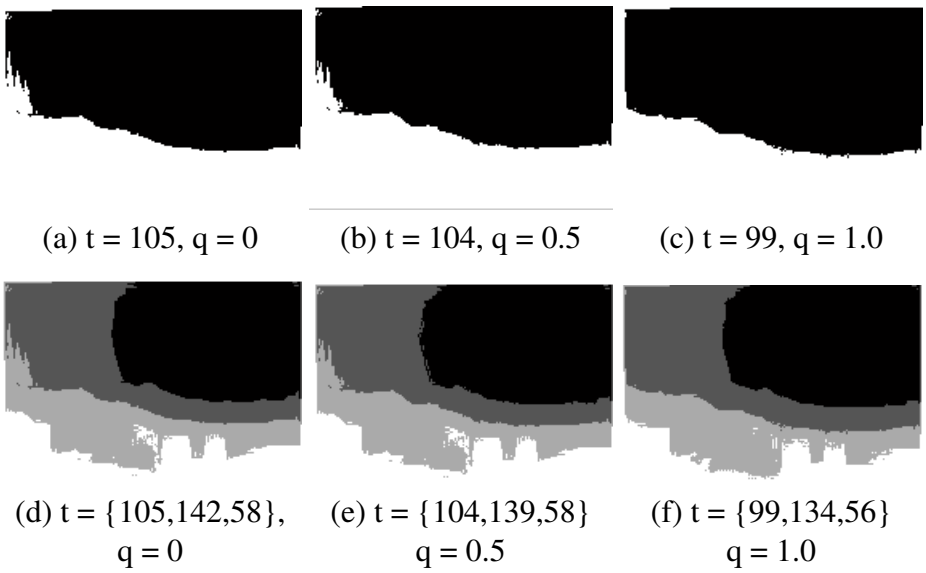

(a) t = 105, q = 0 (b) t = 104, q = 0.5 (c) t = 99, q = 1.0

(d) t = {105,142,58}, q = 0 (e) t = {104,139,58} q = 0.5 (f) t = {99,134,56} q = 1.0

extracting soft as well as hard tissues by searching tumors or defects. In both cases, there is the necessity to extract one from other. Fig. 3a-c shows a segmentation of Fig. 1c for three values of qr with non-recursive Tsallis entropy algorithm.

Sometimes, inside the hard tissue (as well as in soft one), we also need to separate specific parts. It happens when, for example, we should outline some parts of the hard tissue by aligning some possible accidental patient's rotation posed on the bed when MRI is taking. When there is a need of separating such regions, the simple Tsallis entropy segmentation does not work. To show the effectiveness of our approach in this case, we segmented the image of Fig. 1c with NESRA algorithm for three values of q, as can be seen in Fig. 3d-f. The better results, however, were accomplished for $q = 0$. However, the effectiveness of our approach over this kind of image will depend on the desired goal, but, the three segmentation in Fig. 3d-f show the higher flexibility of our proposed method.

The third data set we have used in our experiments are synthetic images from the Columbia database (NENE; NAYAR; MURASE, 1996). As aforementioned, this is an database built to scientific experimentation. It consists of 7200 images of 100 objects at several viewers. Although the object photos had been taken under homogeneous background, which facilitates the foreground extraction, several applications need recognition of object's parts. Then, the application of a simple object segmentation algorithm, as the simple non-recursive Tsallis entropy, does not work well. This fact can be observed in the segmentation of Fig. 1d outlined in Fig. 4a-c. In this figure, the only acceptable segmentation is that of Fig. 4a, when $q = 0$. When $q = 0.5$ and 1.0 the result is clearly inferior. When we apply our proposed method (Figs.4d-f.) we can reach well results for all values of q; however, the best is that of Fig. 4d (q=0).

We tested our proposed algorithm also over the lenna image, with the same previous $q = \{0, 0.5, 1.0\}$ range. We can see the application of the simple extensive algorithm in Fig. 5a-c. By applying the proposed non-extensive algorithm over the same original image, we

Figure 3 – A sequence of segmented head MRI. The first row (images a-c) are the segmentations with the simple non-recursive Tsallis entropy, and the second row (images d-f) are the corresponding segmented with our proposed algorithm. t stands for the achieved threshold. We used $q = \{0, 0.5, 1.0\}$ values.

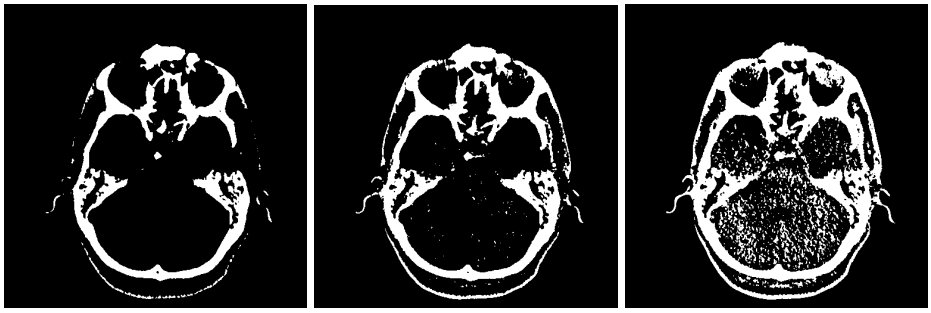

(a) t = 130, q = 0 (b) t = 68, q = 0.5 (c) t = 29, q = 1.0

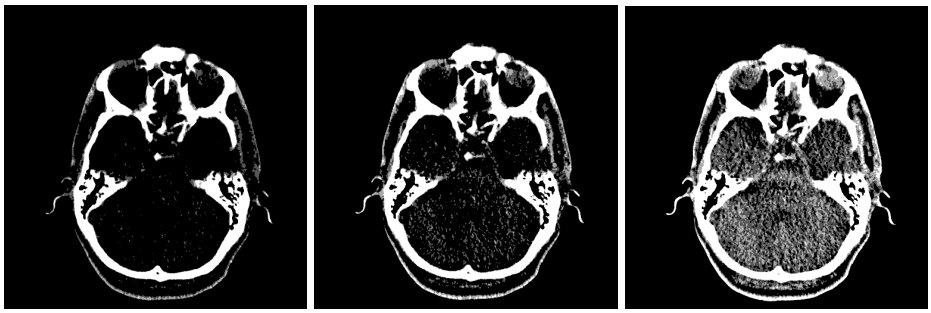

(d) t = {130,201,60}, q = 0 (e) t = {68,144,34}, q = 0.5 (f) t = {29, 78, 6}, q = 1.0

Figure 4 – Segmentation of an image of the Columbia database (Fig. 1.k). The first row shows three segmentations for $q = \{0, 0.5, 1.0\}$. The second row shows the corresponding three segmentations when we applied our proposed method with the same q range.

(a) t = 106 q = 0 (b) t = 138, q = 0.5 (c) t = 138, q = 1.0

(d) t = {106, 151, 62}, q = 0 (e) t = {138,170,90}, q = 0.5 (f) t = {170, 130, 90}, q = 1.0

Figure 5 – The segmentation of lenna image for $q = \{0, 0.5, 1.0\}$. The first row presents the simple non-extensive algorithm and second row presents the corresponding recursive version. t stands for the found threshold value.

(a) t = 129, q = 0 (b) t = 124, q = 0.5 (c) t = 122, q = 1.0

(d) t = {129, 184, 75}, q = 0 (e) t = {124,176,78}, q = 0.5 (f) t = {122, 174, 79}, q = 1.0

reached better results, in terms of segmentation, as can be seen in the corresponding images in Fig. 5d-f. Although in this case just one recursion was applied, generating four different gray scale regions, it is sufficient for a better separation of the main regions than that reached in Fig. 5a-c. The corresponding results can be observed in Fig. 5d-f. Note, for example that the hat's plumage can now be better outlined than before.

Until now, all presented experiments were carried out with no previous filtering application in order to reduce noising. Also, to show a considerable level of image's details, it was sufficient to apply our proposed algorithm with just one level of recursion. It may be an advantage as it yields to a low computational time. However, it is interesting to observe our proposed methodology applied after the application of some gaussian filtering by reducing some noising with once more level of recursion. So, as a final experimentation, we show the application of our proposed algorithm over a painting of a complex scene (Fig. 6a). Before the application of our proposed algorithm we have applied a gaussian filtering and iterate the segmentation two times. The results can be seen in Fig. 6b. This is a well delimited region image with few noising and spurious regions.

In the following we compare our proposed approach with five known algorithms cited in the introduction, namely: bootstrap, fuzzy c-means, k-means, SOM and watershed. In Figures 7 and 8 we have three columns and five rows. Each row corresponds to an image from Figure 1, and each column corresponds to a different method of basic segmentation, namely (from the most left column to the most right column): our proposed NESRA algorithm, boostrap, fuzzy c-means, k-means, SOM and watershed.

Figure 6 – Paint image: (a) is the original image and (b) is its segmentation with q=0 and 3 recursive levels after a gaussian filtering.

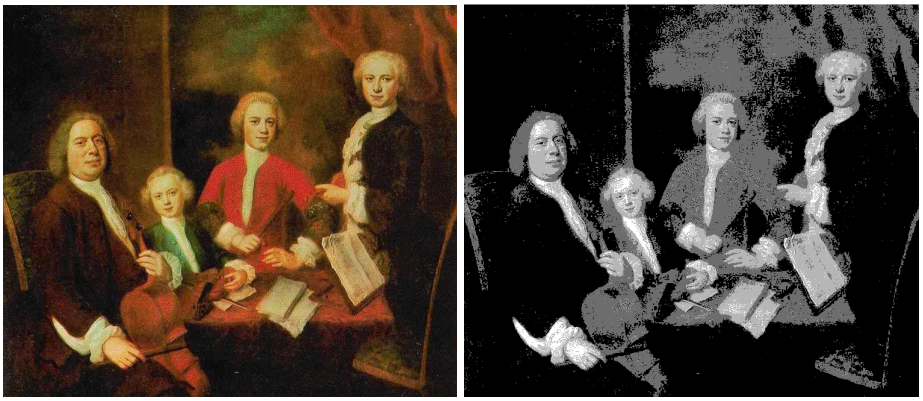

(a) original image (b) segmented

Figure 7 – Results of application of three approaches for image segmentation: column 1: proposed NESRA method; column 2: bootstrap; column 3: fuzzy c-means

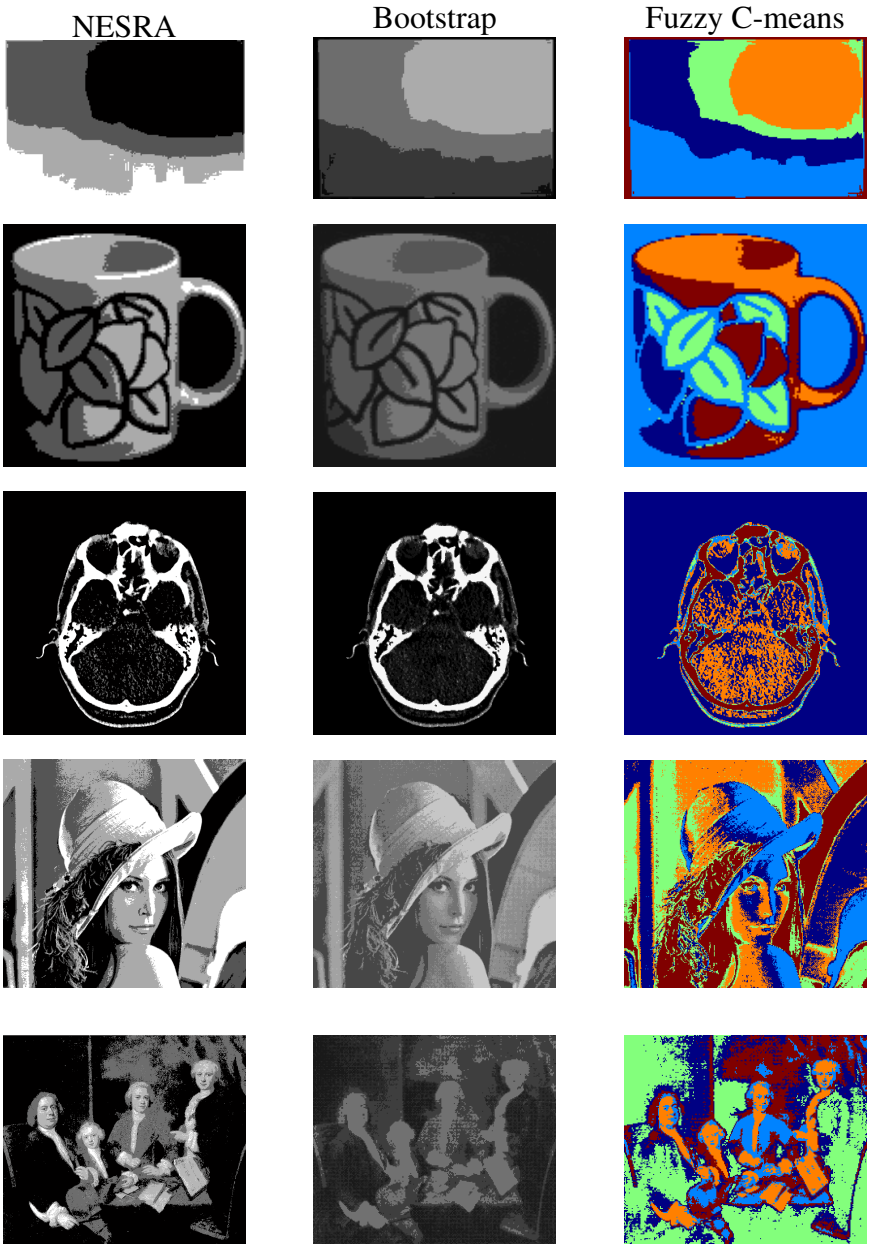

Figure 8 – Results of application of three approaches for image segmentation: column 1: k-means; column 2: SOM; column 3: watershed

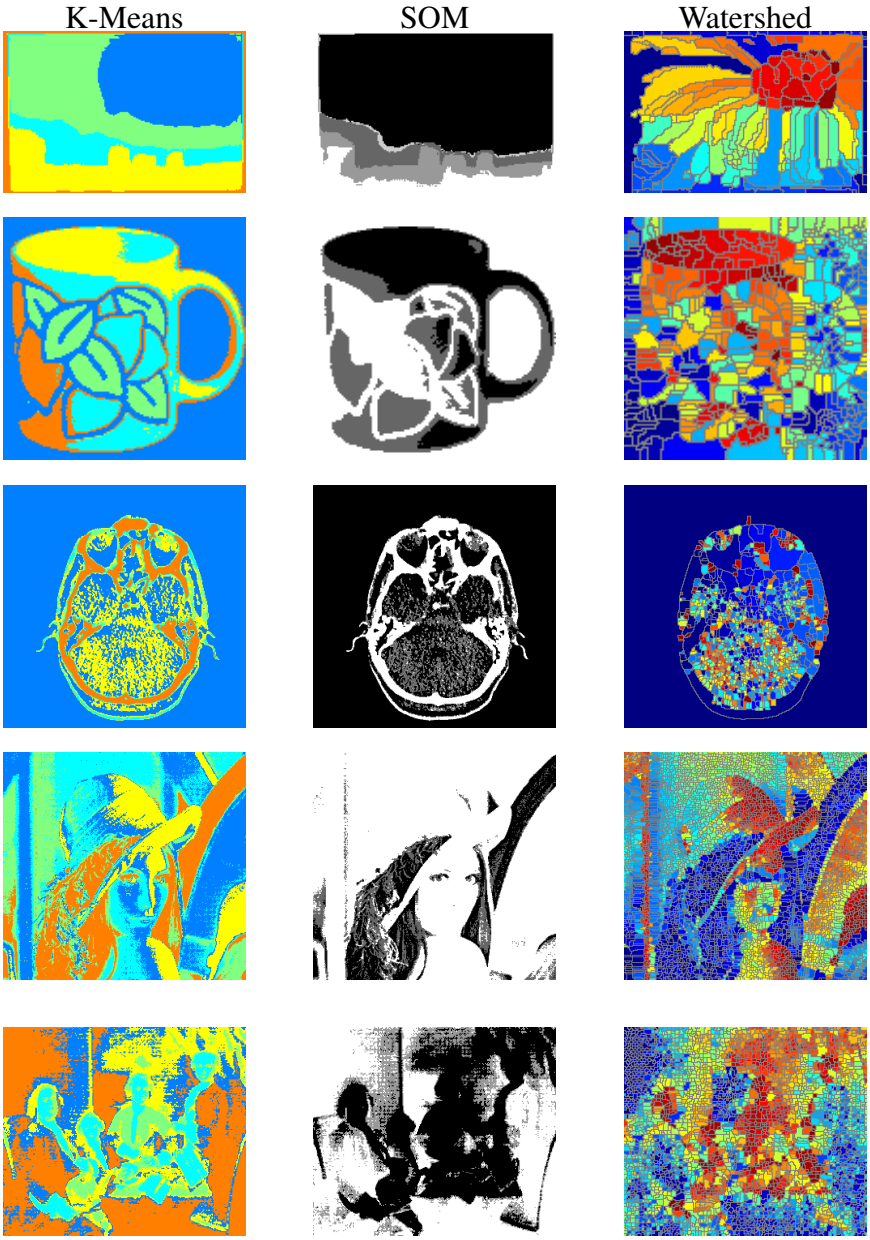

Figure 9 – The synthetic image used to compare the robustness of the methods and increasing application of gaussian noise. The two concentric circles have radius 100 and 50, and the intensities for the background, outer and inner circles are 150, 100 and 50 respectively. The letfmost image is the original image; the three others, from left to right, have $\mu = 0$ and $\sigma^2 = 0.01, 0.05$ and 0.1 gaussian noise respectively.

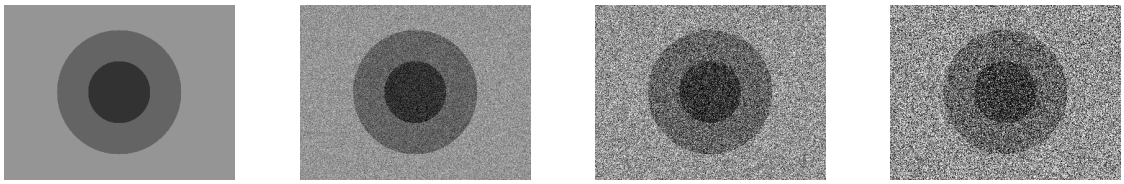

The NESRA was ran with two recursions, which means that there are up to four main regions. Bootstrap was ran in order to achieve up five clusters as well as fuzzy c-means and k-means. On the other hand, we set the SOM network to spread their input data among a 3×2 rectangular grid of neurons, however, similar results were obtained with a 4×4 and 6×6 rectangular grid. Besides, the watershed algorithm was set with an 8-connected approach. Regarding these constraints, we can make the following discussion about the Figures 7 and 8.

In the first row of Figures 7 and 8 (which correspond to Figure 1.a and d) we can see that the NESRA and k-means reach similar results in comparison with Bootstrap, Fuzzy c-mean, SOM and watershed, since NESRA and k-means achieve the four main salient regions, which correspond to light around the sun, sky, horizon and buildings. In particular, NESRA seems to delineate better these four regions.

In the second row (a cup with some drawings with homogeneous background corresponding to Figure 1.d), we can discard only SOM and watershed results (columns 2 and 3 of Figure 8) and analyze only the other four, which seems to generate similar results. Among them fuzzy c-means produced a little bit noise, NESRA and Bootstrap are very similar, and k-means seems to produce a little better segmented main regions.

In the third row of both figures, we have a MRI corresponding to image from Figure 1.c. Now it is difficult to say with no doubt which are the correct mains region (e.g., which are the soft or hard tissue), but generally, the white pixels of Figure 1.c are those corresponding to hard tissue. According to it, only the watershed must be discarded. Among the other four approaches, fuzzy c-means, k-means and SOM oversegmented the images and NESRA and bootstrap seems to separated better the soft tissue.

In the four row of both figures, again, all approach except NASRA and bootstrap oversegmented the images, but NASRA has clearly low noise and homogeneous main regions, as we can see around the lenna's skin and the regions on her right.

In the last row we show a paint figure. This kind of image, generally has high not homogeneous regions with rich texture and colors, then, it is suitable to compare the presented approaches. In this example, NESRA has clearly overcoming all the other methods since it has produced more homogeneous regions with rich level of details (see the people's eyes) well separate one each others.

Finally, in order to quantify a comparison between the methods, we have ran each algorithm with a synthetic image consisting of two concentric circles with radius 100 and 50. The intensities of the background and the outer and inner circler are 150, 100 and 50, respectively. These intensities do not have large distances in their histograms. The experiment consists of applying in this synthetic image a gaussian noise with zero mean and variance $\sigma^2 > 0$. The Figure 9 shows the used synthetic image besides three examples of increasing application of gaussian noise with $\mu = 0$ and $\sigma^2 = 0.01, 0.05$ and 0.1. After, a 2D 9×9 adaptive noise removal filter was applied, which causes noise dropping but blurring the frontiers between the inner and outer circles and the outer circle and the background as well. Although the value of $n = 9$ has been chosen empirically, it is the same for all algorithm in order to put them under the same conditions. Also, in the case of NESRA method, the value of $q = 0.001$ was applied for the synthetic image. This value was chosen empirically and, the good results indicate the system non-extensiveness.

Then, a procedure, based on the Door-In-Door-Out algorithm, was implemented so that to extract the image regions and to obtain the coordinates of the curves for both inner and outer boundaries. Our goal is to measure the robustness of the methods in achieving the original boundaries under increasing values of noise variance. Then, we use the original boundary as a ground truth and compute how far from it is the estimated. The coordinates of the inner and outer original curves were obtained in a straightforward manner by analytical calculation, given their radius and center.

The comparison between an original and an estimated curves was carried out through the PolyLine Distance Measure (PDM) method, proposed by Suri, Haralick and Sheehan (2000), Suri, Setarhedran e Singh (2002), Suri (1998), Suri, Haralick and Sheehan (1996). The PDM is defined as the closest distance from each estimated boundary point to the ideal/ground-truth region of interest boundary. The closest distance of each estimated boundary point can be the perpendicular distance (shortest Euclidian distance) to one skin-line, or can be one of the end boundary points joining the points of the closest interval. It is a measure of the average polyline distance of all boundary points of the estimated and ground-truth curve boundaries. Let B_1 be the first boundary and let B_2 be the second boundary. Then, we can derive the PDM measure, d_{poly}^{Error}, as follows:

$$d_b(A, B_2) = min_{S \in sides B_2} d(A, S) \tag{21}$$

$$d_{vb}(B_1, B_2) = \sum_{A \in vertices B_1} d_b(A, B_2) \tag{22}$$

$$d_{poly}^{Error} = \frac{d_{vb}(B_1, B_2) + d_{vb}(B_2, B_1)}{\sharp vertices \in B_1 + \sharp vertices \in B_2} \tag{23}$$

Also, the PDM Equation (23) does not need the two boundaries B_1 and B_2 having the same length. Note the two main characteristics of the PDM equation: first, as $B_1 \to B_2$, $d_{poly}^{Error} \to 0$; second, it is a distance in pixel units. If $N \times M$ is the image dimension, it is straightforward to

Figure 10 – The result segmentation of the six considered algorithms in this paper. In this illustration, for all the original image we have applied a gaussian noise with zero mean and $\sigma^2 = 0.1$ which is the highest noise used, and after, a 9×9 2D adaptive filter was used for smoothing the noise. In the specific case of NESRA algorithm we use the parameter $q = 0.001$ since it generates the best visual result with more homogeneous and noiseless regions.

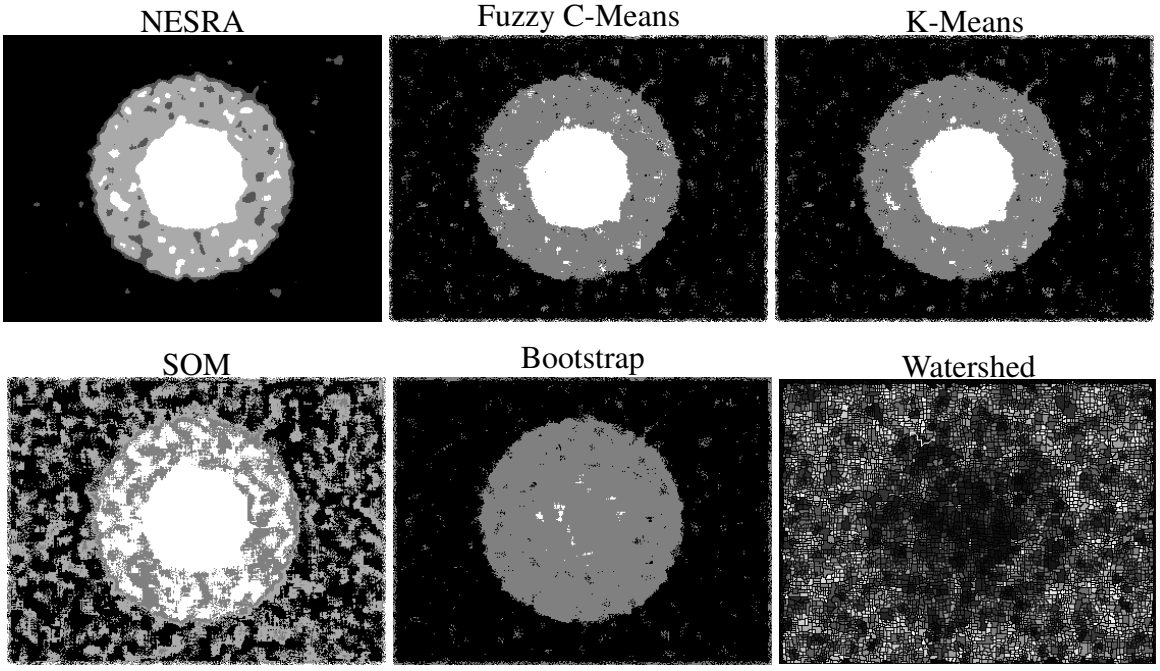

show the maximum value for d_{poly}^{Error} as:

$$d_{max} = |R - r| \tag{24}$$

where R is the larger image's diagonal and r is the average radius of the estimated curve. For a fixed N and M, and dividing (23) by (24), we can define the robustness of an algorithm in achieving the ideal boundary as:

$$R = 1 - \frac{d_{poly}^{Error}}{d_{max}} \tag{25}$$

which is a percentage of the maximum error. Note that $R \to 0$ when the error is maximum and $R \to 1$ when the error is minimum. Therefore, in our experiments, we compute R as a function of increasing values of σ^2 in order to see the general performance of the methods while achieving the ideal boundary. We also compare them under the same conditions and scenarios.

In order to visually compare the methodology's robustness, we superpose the estimated curves on the original images, after applying the 2D adaptive filtering. To give a visual idea of the result, we choose to illustrate this paper with the higher used variance ($\sigma^2 = 0.1$) in the segmented synthetic images. In the Figure 10, we show the segmentation applying in the synthetic for the six methodologies. In this figure, all the segmented image's regions, only for viewing, were assigned to a different gray scale intensity: black for background, gray for outer circle and white for inner circle.

Figure 11 – The estimated (black ones) and original (white ones) curves superimposed over the original image corresponding to the segmentations of Figure 10. Only the watershed was traced manually since we do not have good precision of the boundary in this case.

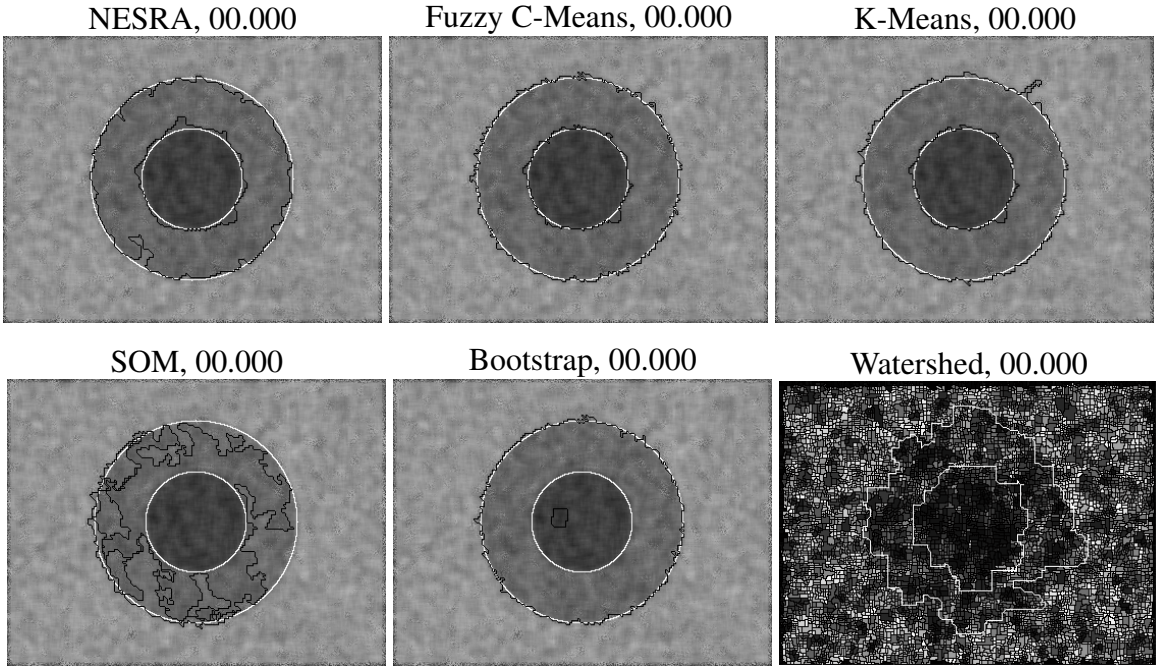

In the Figure 11 we show the original and estimated curves superimposed over the original image after the application of the 2D adaptive filter. In the case of watershed approach, we trace manually the estimated curve since the watershed method oversegment the images, yielding to severe difficulties in boundary extraction. We only show the segmented results and inform that it achieves the bad results among all the compared methods. But we highlight that this is not the conditions to what the watershed works well. To see papers explaining well application of watershed algorithm see (MEYER, 1992) and (GONZALEZ; WOODS, 1992).

A complete numerical result for $\sigma^2 = \{0.01, 0.02, \ldots 0.1\}$ can be see in the Figures 12-left and 12-right, where we plotted R as a function of the complete used range for σ^2. Also,

Figure 12 – Comparative performance of the five used methods as a function of increasing gaussian noise. Left image is for the outer circle and right one is for inner circle. The x-line is the σ^2 and y-line is R according to Equation (25).

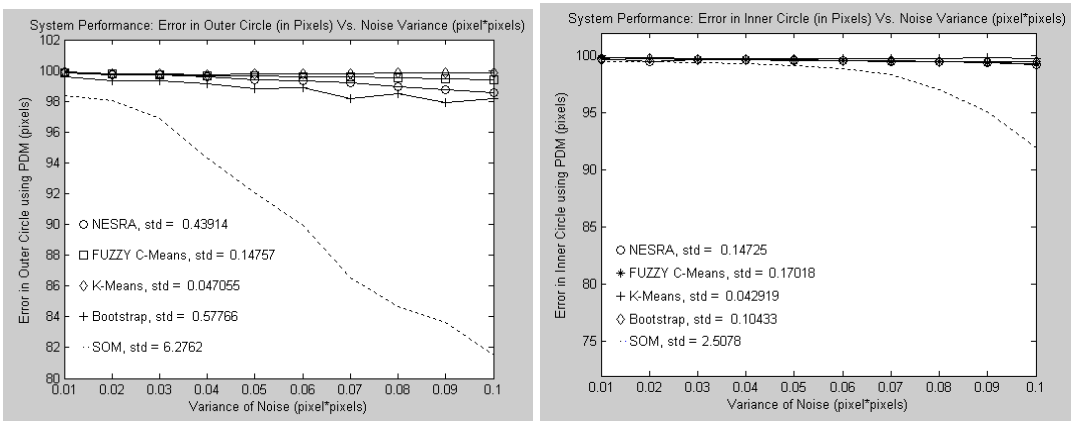

Figure 13 – Comparative performance for the five used methods according to the estimated area inside inner, outer and background regions. The performance percentage is an average of the estimated area of the three regions. The x-line is the σ^2 and y-line is the average of estimated area (for the three regions) divided by real area.

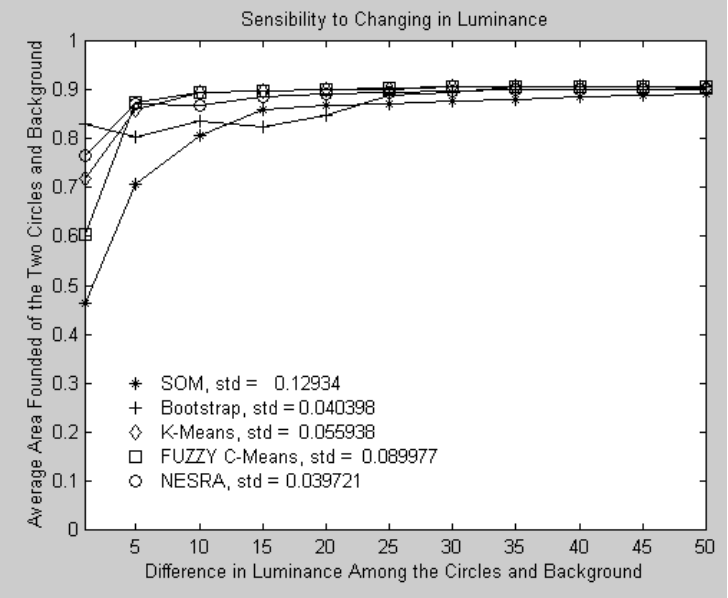

Figure 12 shows the comparative performance for the used algorithms except for watershed method. Figure 12-left shows the results for the outer curve and Figure 12-right does the same for the inner curve of each method.

A final graphic is showed in Figure 13, where we plotted an average percentage of the original area for the inner, outer and background areas as a function of increasing gaussian noise.

The running time of the NESRA algorithm is proportional of the binary procedures, $O(\log N)$, where N is the image dimension. This is due to as we partite the image at each iteration, the number of pixels to be evaluated drops proportionally according to N.

4 Discussion and Conclusion

We have presented a new method for image segmentation based on non-extensive entropy. This new method is a recursive version, called NESRA, of that proposed in (ALBUQUERQUE et al., 2004).

The NESRA algorithm is a segmentation procedure for basic segmentation, which should be used in an initial segmentation. As such, it was compared with other algorithms under the same conditions, namely: Bootstrap, Fuzzy C-Means, K-Means, SOM and Watershed. All of these algorithms were ran for several classes of images, where some examples are in Figure 1, and for a synthetic image, that can be seen in Figure 9.

The proposed algorithm reaches results at least similars to those obtaining the best

performance among three images (sunset, object, MRI) and clearly overcomes the others approaches for lenna and paint image, which may be an indication that this is a good new strategy for image segmentation, or that, by considering an image as a non-extensive system, also is a promisor line of investigation.

The NESRA algorithm obtained more homogeneous and noiseless regions which yields to no oversegmentation images. this is due to the fact that the NESRA always partitions the data set into two new regions, yielding to less sensitiveness to noise and spurious regions.

Regarding the time complexity, although its equations show an exponential growing at each iteration, it is compensated by the dropping of the number of pixels to be evaluated. This time complexity is of the class $\lg N$, where N is the region dimension.

It may be argued that any algorithm for binary segmentation (e.g., such as the well known iterative threshold) may be extended to a recursive version and applied like NESRA. However, it always partitions the luminance space into two blocs, always generating a background and a foreground which maximizes the information. In comparison with the traditional method proposed by Pun (1981), which uses the Shannon entropy, the NESRA overcomes it in all images presented in Figures 2-5. It indicates that the NESRA's advantage is not simply its recursion. Beyond that, a better separation between the foreground and background may be achieved due to the flexibility of the q parameter.

Regarding the choice of the q parameter, an automatic value can not be found yet. Then, as future work, we proposed the investigation of the optimal q through an iterative method, since that the entropic equations are functions of q. At this moment, depending on the class of image, the value of q may be taken from a small discrete range between $0 \leq q \leq 1$. This is the case of all experiments of this paper. As we can see for all results, there is little changing in the results when q varies, since the entropy values depend on mainly from the luminance distribution than the q value. This is one of the indications that we may take advantage in considering images as non-extensive systems.

According to Figure 10, under the maximum gaussian noise ($\sigma^2 = 0.1$), only the methods NESRA, Fuzzy C-Means and K-Means obtained good segmentation. In the cases of the methods Fuzzy and K-Means, they obtained a quite identical results, but both with a hight background noise compared with NESRA. The NESRA and Bootstrap were less sensitive to background noise; however, the NESRA segmented bed the outer region, while the Bootstrap did not achieve any inner circle. On the other hand, the SOM and the Watershed had a oversegmentation. Similar results also can be seen in the Figure 11, where the NESRA, Fuzzy C-Means and K-Means are compatible in achieving the boundaries. The contrary occurs with the SOM, Bootstrap and Watershed. In this case, only the Bootstrap found the central circle.

When these results are quantitatively analyzed, as observed in the Figure 12 and 13, both Fuzzy C-Means and K-Means, as well as NESRA, were stable with slight advantage to Fuzzy C-Means and K-Means, in achieving the inner circle. On the other hand, also the Bootstrap was stable in achieving the outer circle (Figure 12-left) but had low performance in achieving the inner circle (Figure 12-right).

When we compare the estimated areas with the original ones (Figure 13) the performance of all algorithms are quite similars. The Fuzzy C-Means and K-Means have similar good performance and NESRA are compatible with them, while SOM, Bootstrap and Watershed have low performance.

Finally, we can conclude that the NESRA algorithm has compatible performance with the best tested algorithms for the synthetic image and better performance of all methods in real images when analyzed qualitatively. This is due to the NESRA algorithm reaches a better homogeneity of the target regions. It was less sensitive to noise than all the others methods with the aditional advantage of low time complexity. Then, NESRA algorithm is well indicated to segment general images even at real time.

In the future, we will test NESRA algorithm inside a complete system for image segmentation, possible applying, after an initial segmentation, the active contour models in order to smooth the found boundaries. Also, a possible future direction is to study the best class of images to apply the NESRA methodology. The best class can be defined though the ideal q value.

ACKNOWLEDGMENT

The authors are grateful to CAPES (Coordenação deAperfeiçoamento de Pessoal de Nível Superior) and CNPq (Conselho Nacional de Desenvolvimento Científico e Tecnológico), Brazilian agencies for Scientific Financing, for the support of this work.

REFERENCES

ABUTALEB, A. S. A new method for gray-level picture thresholding using the entropy of the histogram. **Comput. Graphics Image Process**, v. 47, p. 22–32, 1989.

ALBUQUERQUE, M. P. et al. Image thresholding using tsallis entropy. **Pattern Recognition Letters**, v. 25, p. 1059–1065, 2004.

BEZDEK, J. C. **Fuzzy Mathematics in Pattern Classification**. 1973. Tese (Doutorado) — Cornell University, Ithaca, NY, USA.

BEZDEK, J. C. Partition structures: A tutorial. In: **The Analysis of Fuzzy Information**. Boca Raton, FL: CRC Press, 1987.

CHEN, C. W.; LUO, J.; PARKER, K. J. Image segmentation via adaptive k-mean clustering and knowledge-based morphological operations with biomedical applications. **IEEE Transactions on Image Processing**, v. 7, n. 12, p. 1673–1683, Dec. 1998.

CHEN, D.R. et al. Use of the bootstrap technique with small training sets for computer-aided diagnosis in breast ultrasound. **Ultrasound Med. Biol.**, v. 28, n. 7, p. 897–902, July 2002.

COMANICIU, D.; MEER, P. Mean shift: a robust approach toward feature space analysis. **Pattern Analysis and Machine Intelligence, IEEE Transactions on**, v. 24, n. 5, p. 603–619, 2002.

DAVE, R. N.; BHASWAN, K. Adaptive fuzzy c-shells clustering and detection of ellipses. **IEEE Transactions on Neural Networks**, v. 3, n. 5, p. 643–642, 1992.

DONG, G.; XIE, M. Color clustering and learning for image segmentation based on neural networks. **IEEE Transactions on Neural Networks**, v. 16, n. 4, p. 925–936, July 2005.

DUNN, J. C. A fuzzy relative of the isodata process and its use in detecting compact, well-separated cluster. **Journal of Cybernetics**, v. 3, p. 32–57, 1974.

DUTENDAS, D. et al. Unsupervised bayesian segmentation with bootstrap sampling application to eye fundus image coding. In: NUCLEAR SCIENCE SYMPOSIUM AND MEDICAL IMAGING CONFERENCE, 1994. **IEEE Conference Record**. Norfolk, 1994. v. 4, p. 1794 – 1796.

GOKTEPE, M.; YALABIK, N.; ATALAY, V. Unsupervised segmentation of gray level markov model textures with hierarchical self organizing maps. In: INTERNATIONAL CONFERENCE ON PATTERN RECOGNITION, 3, 1996. **Proceedings...** USA, 1996. v. 4, p. 90–94.

GONZALEZ, R. C.; WOODS, R. E. **Digital Image Processing**. Reading, MA: Addison Wesley, 1992.

GRAY, R. M.; LINDE, Y. Vector quantization and predictive quantizers for gauss-markov sources. **IEEE Transactions on Communications**, v. 30, n. 2, p. 381–389, February 1982.

KAPUR, J. N.; SAHOO, P. K.; WONG, A. K. C. A new method for gray-level picture thresholding using the entropy of the histogram. **Comput. Graphics Image Process**, v. 29, p. 273–285, 1985.

KOHONEN, T. **Self-Organizing and Associated Memory**. 3rd. ed. New York: Springer-Verlag, 1989.

KRISHNAPURAM, R.; NASRAOUI, O.; KELLER, J. The fuzzy c spherical shells algorithm: A new approach. IEEE trans. neural networks. **IEEE Transaction on Neural Networks**, v. 3, n. 5, p. 663–671, 1992.

KURNAZ, M. N.; DOKUR, Z.; OLMEZ, T. Segmentation of ultrasound images by using an incremental self-organized map. In: ANNUAL INTERNATIONAL CONFERENCE, 23, 2001. **Proceedings of the IEEE Engineering in Medicine and Biology Society**. Istanbul, Turkey, 2001. v. 3, p. 2638–2640.

LI, C. H.; LEE, C. K. Minimum cross entropy thresholding. **Pattern Recognition**, v. 26, p. 617–625, 1993.

LI, N.; LI, Y. Feature encoding for unsupervised segmentation of color images. **IEEE Transactions on Systems Man and Sybernetics - Part B: Cybernetics**, v. 33, n. 3, p. 438–447, June 2003.

LOHMANN, G. **Volumetric Image Analysis**. Chichester: Wiley, 1998.

LUO, M.; YU-FEI, M.; HONG-JIANG, Z. A spatial constrained k-means approach to image segmentation. In: IEEE JOINT CONFERENCE OF THE INTERNATIONAL CONFERENCE ON INTERNATIONAL CONFERENCE ON INFORMATION, COMMUNICATION AND SIGNAL PROCESSING, AND PACIFIC RIM CONFERENCE ON MULTIMEDIA, 2003. **Proceedings...** Singapore, 2003. v. 2, n. 4, p. 738–742.

LUO, Q.; KHOSHGOFTAAR, T. M. Efficient image segmentation by mean shift clustering and mdl-guided region merging. In: IEEE INTERNATIONAL CONFERENCE ON TOOLS WITH ARTIFICIAL INTELLIGENCE ICTAI, 16, 2004. **Proceedings of the Nuclear Science Symposium and Medical Imaging Conference**. Boca Raton, Florida, 2004. v. 4, p. 337–343.

MA, F. et al. Probabilistic segmentation of volume data for visualization using som-pnn classifier. In: IEEE SYMPOSIUM ON VOLUME VISUALIZATION, 1998. **Proceedings...** Research Triangle Park, NC, USA, 1998. v. 3, p. 71–78.

MAKROGIANNIS, S.; ECONOMOU, G.; FOTOPOULOS, S. A region dissimilarity relation that combines feature-space and spatial information for color image segmentation. **IEEE Transactions on Systems Man and Sybernetics - Part B: Cybernetics**, v. 35, n. 1, p. 44–53, Feb. 2005.

MAKROGIANNIS, S. et al. Segmentation of color images using multiscale clustering and graph theoretic region sysntesis. **IEEE Transactions on Systems Man and Sybernetics - Part A: Systems and Humans**, v. 35, n. 2, p. 224–238, Mar. 2005.

MARSHALL, I. Kochand G. Bootstrap coverage plots for image segmentation. In: 13TH INTERNATIONAL CONFERENCE ON PATTERN RECOGNITION, 1996. **Proceedings...** Vienna, 1996. v. 2, n. 2, p. 447–451.

MEYER, F. Color image segmentation. In: IEEE CONFERENCE ON IMAGE PROCESSING AND ITS APPLICATIONS, 4, 1992. **Proceedings...** Maastricht, 1992. v. 354, n. 53, p. 303–306.

NENE, Sameer A.; NAYAR, ShreeK.; MURASE, Hiroshi. **Columbia object image library (coil-100)**. Department of Computer Science. New York, 1996. Retrieved May 29, 2013, from <http://www1.cs.columbia.edu/CAVE/publications/pdfs/Nene_TR96_2.pdf>.

PAL, N. R. On minimum cross entropy thresholding. **Pattern Recognition**, v. 26, p. 575–580, 1996.

PAPPAS, T. N. An adaptative clustering algorithm for image segmentation. **IEEE Transactions on Signal Processing**, v. 40, n. 4, p. 901–914, April 1992.

PUN, T. Entropic thresholding: A new approach. **Comput. Graphics Image Process**, v. 16, p. 210–239, 1981.

RICKARD, H. E. et al. Breast segmentation in screening mammograms using multiscale analysis and self-organizing maps. In: ANNUAL INTERNATIONAL CONFERENCE OF THE ENGINEERING IN MEDICINE AND BIOLOGY SOCIETY (EMBC), 26, 2004. **Proceedings...** San Francisco, Calif, USA, 2004. v. 1, p. 1786–1789.

RONG-CHUN, Feng Wei;. Non-rigid objects detection and segmentation in video sequence using 3d mean shift analysis. In: INTERNATIONAL CONFERENCE ON MACHINE LEARNING AND CYBERNETICS, 2003. **Proceedings ...** Xi-an, China, 2003. v. 5, p. 3134–3139.

SAHOO, P. K.; SOLTANI, S.; WONG, A. K. C. A survey of thresholding techiniques. **Comput. Vis. Graphics Image Process**, v. 41, p. 233–260, 1988.

SHAH-HOSSEINI, H.; SAFABAKHSH, R. Automatic multilevel thresholding for image segmentation by the growing time adaptive self-organizing map. **IEEE Transactions on Pattern Analysis and Machine Intelligence**, v. 24, n. 10, p. 1388–1393, Oct. 2002.

SHANNON, C.; WEAVER, W. **The Mathematical Theory of Communication**. Urbana: University of Illinois Press, 1948.

SINGH, M. et al. Segmentation of functional mri by k-means clustering. **IEEE Transactions on Nuclear Science**, v. 43, n. 3, Part 2, p. 2030–2036, June 1996.

SURI, J. Error and shape measurement tools for cardiac projection images: a closer look. In: INTERNATIONAL CONFERENCE IN APPLICATIONS OF PATTERNS RECOGNITION, 1998. **Proceedings ...** Plymouth, England, 1998. v. 4, n. 1, p. 125–134.

SURI, J.; HARALICK, R. M.; SHEEHAN, F. H. Greedy algorithm for error reduction in automatically produced boundaries from low contrast ventriculogram. In: INTERNATIONAL CONFERENCE IN PATTERN RECOGNITION (ICPR), 1996. **Proceedings ...** Viena, Austria, 1996. v. 4, n. 1, p. 361–365.

SURI, J.; HARALICK, R. M.; SHEEHAN, F. H. Greedy algorithm for error reduction in automatically produced boundaries from low contrast ventriculogram. **International Journal of Pattern Analysis and Applications**, v. 3, n. 1, p. 39–60, 2000.

SURI, J.; SETARHEDRAN, S. K.; SINGH, S. **Advanced algorithm approaches to medical image segmenttion: state of art applications in cardiology, neurology, mamography and pathology**. New York: Springer-Verlag, 2002.

TSALLIS, C. Nonextensive statistics: Theoretical, experimental and computational evidences and connections. **Brazilian Journal of Physics**, v. 29, n. 1, Mar. 1999.

TSALLIS, C. **Nonextensive Statistical Mechanics and its Applications**. Berlin: Springer, 2001.

XIAN-JIU, G.; WEI, W. Multiscale segmentation algorithm based on subdivision and mean shift. In: INTERNATIONAL CONFERENCE ON MACHINE LEARNING AND CYBERNETICS, 2005. **Proceedings ...** Guangzhou, China, 2005. v. 7, p. 4427–4431.

YAMANO, T. Information theory based in nonadditive information content. **Entropy**, n. 3, p. 280–292, 2001.

ZHENG, T.; XIAN-BIN, W.; WEI, L. Multiscale segmentation of SAR imagery with bootstrap sampling. In: INTERNATIONAL CONFERENCE ON SIGNAL PROCESSING (ICSP), 7, 2004. **Proceedings ...** Beijing, China, 2004. v. 1, p. 713–716.